12-μm OBSERVATIONS AT THE 1991 ECLIPSE

D. E. JENNINGS and D. DEMING
Code 693, NASA/Goddard Space Flight Center, Greenbelt, MD 20771, U.S.A.
G. McCABE
Hughes/STX Corporation, Lanham, MD, U.S.A.
R. NOYES
Harvard-Smithsonian Center for Astrophysics, 60 Garden Street, Cambridge, MA 02138, U.S.A.
G. WIEDEMANN
European Southern Observatory, Karl-Schwarzschildstrasse 2, D-8046 Garching bei München, Germany
and
F. ESPENAK
Code 693, NASA/Goddard Space Flight Center, Greenbelt, MD 20771, U.S.A.

Abstract. The 11 July 1991 total solar eclipse over Mauna Kea was a unique opportunity to study the limb profile of the 12.32 μm MgI emission line. Our observations used the NASA 3-meter Infrared Telescope Facility,[1] and a new Goddard large cryogenic grating spectrometer. Spectra of the line were taken in the slitless mode at second contact. The results show that the emission peaks within $\sim$ 300 km of the 12-μm continuum limb. This agrees with recent theoretical predictions for this line as a NLTE upper photospheric emission feature. However, the increase in optical depth for this extreme limb-viewing situation means that most of the observed emission arises from above $T_{\min}$, and we find that this emission is extended to altitudes well in excess of the model predictions. The line emission can be traced to altitudes as high as 2000 km above the 12-μm continuum limb, whereas theory predicts it to remain observable no higher than 500 km above the continuum limb. The substantial limb-extension observed in this line is qualitatively consistent with limb-extensions seen by other observers in the far-IR continuum, and may be indicative of departures from gravitational hydrostatic equilibrium in the upper solar atmosphere, and/or may result from temperature and density inhomogeneities. The extended altitude of formation of this line enhances its value as a Zeeman probe of magnetic fields.

Key words: eclipses – infrared: stars – Mg I – Sun: atmosphere

1. Introduction

The Mg I emission lines near 12 μm are the most Zeeman-sensitive lines presently observed in the solar spectrum, and of great potential in studies of solar and stellar magnetic and electric fields – Deming *et al.* 1988, Chang and Schoenfeld (1991). First observed by Brault and Noyes (1983), they were originally believed to be formed in the low chromosphere. Early models of the line formation process showed that the emission lines were, in fact probably photospheric in origin (Lemke and Holweger 1987). Whereas Zirin and Popp (1989) argued for chromospheric formation, recent theoretical work (Hoang-Binh 1991, Chang *et al.* 1991, and Carlsson *et al.* 1991, hereafter CRS) strongly suggests that the lines are formed by departures from LTE in the upper photosphere. Indirect evidence from observations of

[1] The Infrared Telescope Facility is operated by the University of Hawaii Institute for Astronomy, under contract with the National Aeronautics and Space Administration. The authors were Visiting Astronomers at this Facility.

D. M. Rabin et al. (eds.), Infrared Solar Physics, 151–160.

https://doi.org/10.1017/S0074180900124374 Published online by Cambridge University Press

the 12.32-μm line – Deming *et al.* (1988) – puts the region of formation near the temperature minimum, as predicted by the recent theory. It is important, however, to show by direct observation that the line is photospheric. Such observations are not possible under normal observing conditions because the spatial resolution attainable with existing solar telescopes at 12 μm is not adequate. The telescope limitations can be exceeded, however, by observing the line intensity during an eclipse using the motion of the lunar limb to obtain very high spatial resolution. We report such observations here, obtained using slitless IR spectroscopy of the 12.3 μm line at the solar limb during the 11 July 1991 total eclipse – Deming *et al.* (1992).

2. Observations

The 3-meter NASA Infrared Telescope Facility (IRTF) on Mauna Kea was used to observe the 12.3 μm line at the solar limb. A high-resolution cryogenic array grating spectrometer, developed at Goddard for planetary and astrophysical applications, was adapted for this experiment. This instrument, which we call Celeste, is shown schematically in Figure 1. The spectrometer was mounted at the Cassegrain focus of the telescope. The grating and all other internal optics in the instrument are cooled with LHe. The beam enters through a lens (which is also the dewar window) and is focussed through two filter wheels at an aperture wheel. The beam passes through a hole in the center of the primary mirror (M3) and has its pupil imaged near the secondary (M2). The Cassegrain secondary and primary mirrors expand the beam before it strikes the grating. The diffracted beam from the grating is refocussed through the center of the primary. A fixed sphere (M4) at the focus sends the beam to a tiltable sphere (M5) located next to the secondary. The angle of this final sphere can be adjusted to return the beam to the grating via the fixed sphere and the secondary, and this multi-pass cycle can be repeated up to three times. For the eclipse, Celeste used a 15×30 cm^2 grating with 31.6 lines mm^{-1}, which was illuminated by a 12.5-cm diameter beam in 4th order. For the eclipse observations, single-pass was used, and the tiltable mirror imaged the beam at the detector array. The detector array was a 10×50 element blocked impurity band (BIB) device. A 386 PC computer controlled the array, stored the data, and communicated with the telescope computer.

Observations were planned for both second and third contact, with telescope motion directed by data computer. Excellent data were obtained at second contact (east limb). Unfortunately, third contact was missed due to a communication failure between the data computer and the telescope control system.

We began preparing Celeste at the observatory one week before the eclipse. However, because of problems with operating the arrays which were solved on the last day, we were not able to mount the instrument on the telescope until approximately six hours before the eclipse. During resolution of the problems, we had to disconnect the internal focus adjustment. The input focus was set to a nominal value based on prior experience in the laboratory. Because we were operating in the slitless mode, where the eclipse edge effectively created our entrance slit, the focus position was not critical. Since the eclipse was an early-morning event, we had only

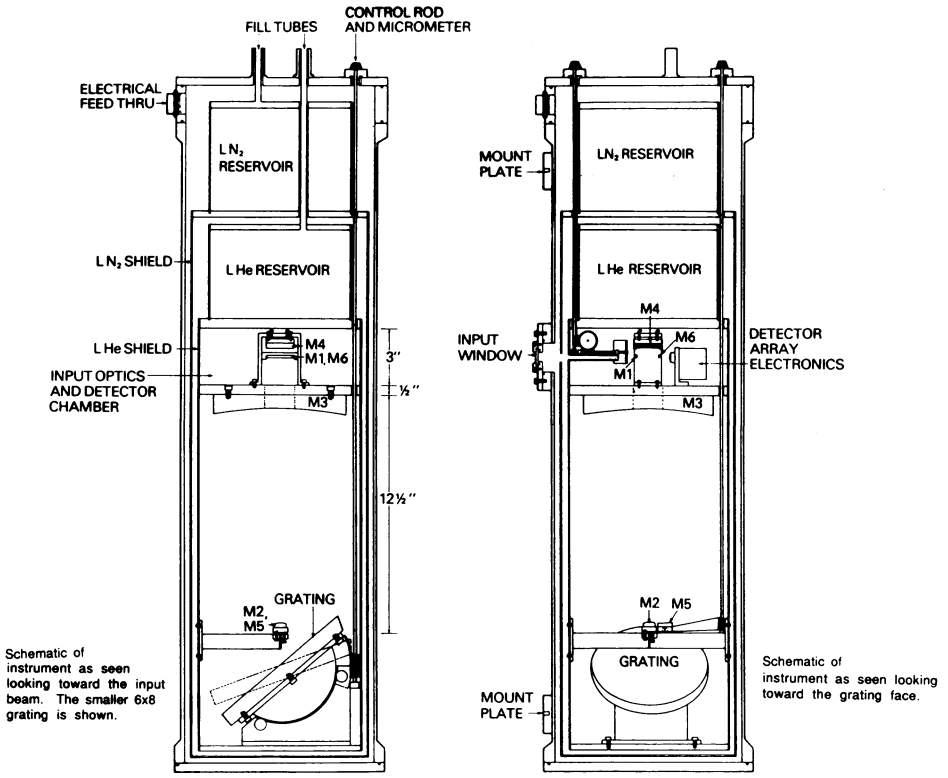

Fig. 1. The cryogenic grating spectrometer, "Celeste", shown schematically. Radiation is focussed by the window/lens, through two filter wheels (fixed and CVF) at an aperture wheel. The beam then is expanded by the Cassegrain system and sent to the 18×33 cm^2 grating (a 15×30 cm^2 grating was used for the eclipse). The diffracted beam is refocussed and transferred by a pair of multi-pass mirrors (used in single-pass) to a final focus at the 10×50 element BIB detector array.

45 minutes available from the time we could first acquire the sun, until second contact at 7:28 AM local time (the eclipse had begun when we first saw the sun!). We set the telescope focus from IRTF documentation, based on the measured position of the Celeste entrance aperture. This left only two adjustments to be made using sunlight: 1) positioning the telescope at the extreme solar limb, and 2) adjusting the grating angle to center the emission line on the detector array. The line was found and centered by first scanning the grating around the previously calibrated position of the line. Limb-brightening of the line was verified by moving the telescope from the limb to a position well on the disk. The resultant grating angle agreed exactly with the prior calibration made using an NH_3 gas absorption cell in the laboratory at GSFC. A cold entrance slit was used in Celeste during the line centering and limb positioning, but the aperture wheel was rotated to the slitless position for the eclipse.

https://doi.org/10.1017/S0074180900124374 Published online by Cambridge University Press

The 3-meter telescope aperture was covered with white polypropylene plastic of a variety used for food packaging; we discovered the material by recording the infrared spectrum of a potato chip bag. The polypropylene absorbed and scattered the visible and near-IR radiation enough to prevent damage to the telescope and instrument optics from focussed sunlight. However, at 12 μm the polypropylene was transmissive without significant scattering, allowing the limb to be observed during the setup phase. The polypropylene was removed about 40 seconds before second contact. We observed the second contact limb at the celestial easternmost point of the disk. This point was found by moving east along the bisector of a north-south chord, and we estimate that the uncertainty in the limb positioning was about 5 arcsec. The east-west positioning could be checked in the observed data by measuring the shift of the line peak with respect to the center of the array. This shift was found to be 8 arcsec.

Several cold entrance apertures are selectable in Celeste. We elected to use a slitless mode for the actual observations, choosing a rectangular aperture which projected to 6×20 arcsec^2 on the sky. We oriented the aperture and array with their long axis perpendicular to the solar limb, and the spectral dispersion was along the long (50-pixel) axis of the array. The rationale for slitless operation was to make sure that the limb was captured within the aperture at second contact, to maximize the signal-to-noise ratio by eliminating the losses which occur using an entrance slit, and to possibly sample more than a single location along the limb (this latter advantage was not realized in practice.) Our concern about the signal-to-noise ratio reflects the facts that the solar intensity is much reduced in the 12-μm region, as compared to the visible, and that high temporal and spatial resolution were needed. Even so, it was necessary to read and co-add at the maximum rate to minimize saturation of the array. Each integration was the result of co-adding approximately 50 frames of the array, which was read at 250 Hz, the maximum rate possible with our data system. The observations consisted of a sequence of 150 consecutive measurements, each consisting of 0.2 second integration plus 0.12 second of overhead. Since the lunar limb motion was 0.53 arcsec sec^{-1}, the spatial resolution normal to the solar limb could be as high as 0.15 arcsec. No sky chopping was used. After second contact, the thermal background level on the moon was measured at the center of the lunar disk, and after third contact flat-field calibration of the array response was performed on the dome wall and with the entrance aperture blocked with warm sources (hand, soldering iron).

3. Data Reduction

Each frame of data was processed by subtracting a lunar background frame (a small contribution), and dividing by a flat-field frame. Inspection of the data after this process reveals that the line emission is about an order-of-magnitude broader than the expected 0.03 cm^{-1} diffraction-limited resolution. This is not altogether surprising, since we were running in slitless mode and had had no opportunity to check the telescope focus. Seeing and defocussing probably account for most of the degraded resolution. Resolution was not critical in this experiment, however, since we only needed to be able to distinguish the line from the continuum. An

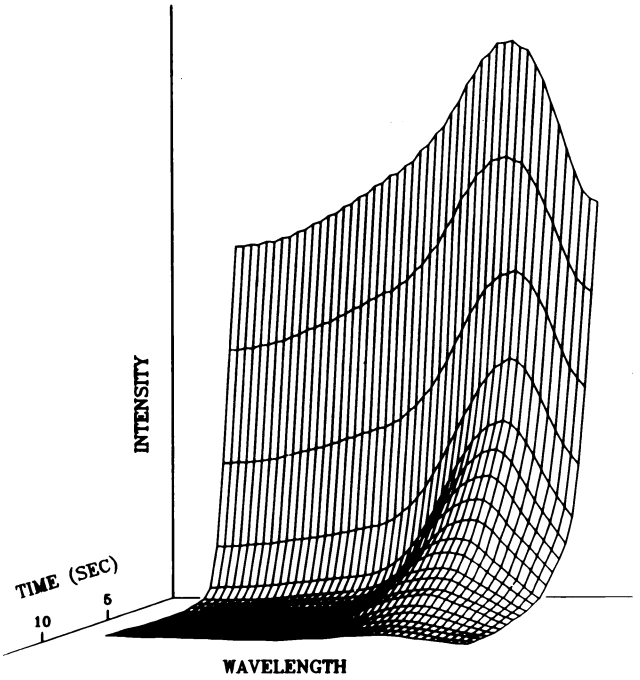

Fig. 2. Spectral data for the 12.32 μm line near second contact, in a 3-D representation. Wavelength increases to the left, frequency increases to the right, with 0.02 cm^{-1} per point. The time scale is equivalent to height in the solar atmosphere, 390 km per second of lunar limb motion), and the vertical axis is relative intensity. The first two detector columns were not operational, so only 48 columns are illustrated.

additional, possibly related, characterisic of the reduced data is that each of the 10 rows of the array gives essentially identical results for the timing of the line and continuum disappearance, consistent with a spatial resolution comparable to the 6 arcsec extent of the array.

Since there seems to be no difference in timing of the eclipse along columns of the array, we averaged along columns to produce a single line spectrum for each frame. The resulting time sequence at second contact is illustrated in Figure 2. The wavelength axis represents the column number of the array, and corresponds to spectral dispersion (0.02 cm^{-1} per column). The intensity axis corresponds to the average in each column of the array. The remaining axis is time, and 21 successive integrations are shown by the lines across the surface at equally spaced time intervals. The continuum radiation from the solar limb in the 1.0 cm^{-1} bandpass of the spectrometer was sufficient to saturate the array until a few seconds before second contact. Figure 2 represents about 7 seconds of data, corresponding to only a few arcseconds of lunar limb motion. The portion of the data near zero on the

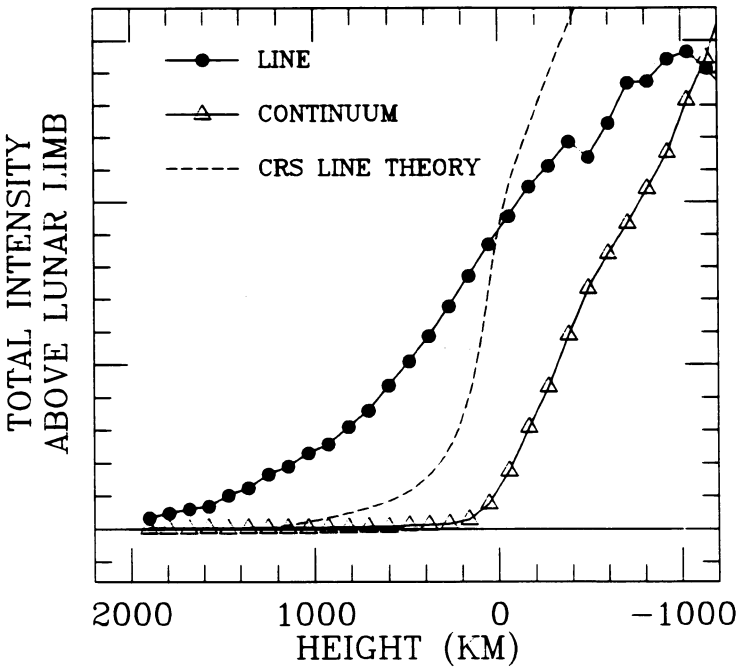

Fig. 3. Observed continuum and 12.32 μm line signal above the height of the lunar limb. The line signal is the total line energy, obtained by integrating the data over wavelength, shown in comparison to the variation predicted by the CRS theory. Height zero is defined to occur at the 12.3-μm continuum limb, and the line and continuum signals are on different relative intensity scales (see text).

time-axis origin is representative of the 12 μm continuum, which drops rapidly to zero at second contact. The emission line is the "ridge" structure apparent in the figure (peaking near column 38); *the line can be observed for up to 5 seconds following the disappearance of the continuum.* Its position on the wavelength scale in Figure 2 is a consequence of the east-west spatial position of the limb within the slitless aperture. In order to derive timing information about the visibility of the line, we averaged the intensity of the line over its profile in each frame. We made no attempt to correct for the fraction of line emission which missed the array on the right in Figure 2. The wavelength-integrated line signal, and the continuum signal, are shown versus time in Figure 3. The line signal was derived by subtracting a continuum contribution from the total flat-fielded array signal. The continuum contribution was calculated by taking column 3 of the flat-fielded array (the leftmost point on Figure 2) as representative of the continuum level, and assuming it to be constant with wavelength. Since the relevant data span only a few seconds of time,

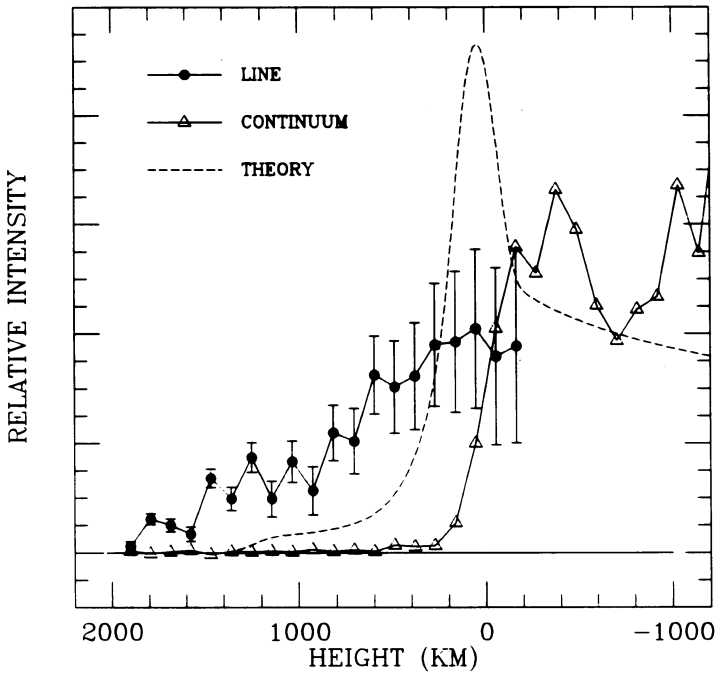

Fig. 4. High resolution limb profiles for the line and continuum, obtained by differencing the Figure 3 data. The dashed line shows the extreme limb profile expected for the total line intensity, computed using the CRS line formation theory, and convolved to the 220 km resolution of the observations. The line and continuum relative intensity scales are different by factor of 10.

the line position does not shift appreciably on the array, and the relative shape of the limb emission profile is unaffected by the fraction of the total line intensity which is missed. The Figure 3 line and continuum data are plotted on different relative intensity scales so that they can be compared more easily; the intensity scale for the line energy is expanded by a factor of 10 from the continuum scale. Also illustrated on Figure 3 is a simulation of the total line energy expected versus time, based on the CRS theory.

The data in Figures 2 and 3 measure the total intensity from regions remaining uncovered by the lunar limb. By taking the difference between successive scans, the intensity due to the portion of the limb covered during the corresponding approximately 0.3 second elapsed time can be derived. The differenced data represents a high spatial resolution scan of the solar limb. The differenced series for our data are shown on Figure 4 for both the line and continuum signals. The height in Figure 4 is defined to be zero at the 12-μm continuum limb; the visible continuum limb is at −400 km on this scale (Chang *et al.* 1991). Noise due to atmospheric fluctuations is

https://doi.org/10.1017/S0074180900124374 Published online by Cambridge University Press

present in the total signals (Figure 3), and becomes more evident in the differenced data (Figure 4). The noise in the original data (Figure 2) can be estimated by the departures of individual values from a smooth (*e.g.*, linear) temporal variation; these fluctuations are typically 3% of the total signal, and occur primarily on a "slow" time scale (typically one to several seconds). Before second contact, when the total signal, dominated by continuum, is largest, its noise fluctuations can result in prohibitively large errors in the differenced line signal. We therefore only plot emission points according to the criterion that the differenced line signal must be larger than a 3% fluctuation in the total signal. This limits us to points at and above the continuum limb (Figure 4). The error bars shown were calculated by assuming that the emission is itself affected by 3% sky-transparency fluctuations, as well as by statistical fluctuations in the thermal background emission. Near the limb, the error bars exceed the fluctuations in the observed points, which is likely due to the fact that the differencing removes much of the relatively slow transparency fluctuations. Well above the limb, the error bars are dominated by statisical background fluctuations, and the fact that the observations show scatter in excess of the errors indicates either that real structure is being observed, or that our estimate of errors is too small in this regime.

In order to estimate the extent of degradation in spatial resolution caused by the irregularity of the moon's limb, we used the charts of Watts (1963) to calculate the range of heights which might be present due to lunar topography, including libration for the summit of Mauna Kea. The relevant topography has a range of heights corresponding to a variation of 0.3 arcsec over our 6-arcsec aperture width. We therefore assume that our height resolution of the solar atmosphere is about 220 km, and this is consistent with the appearance of the 12-μm continuum limb in Figure 4.

The theoretical limb profile of the emission from the CRS theory, accounting for the sphericity of the emitting layers at the extreme limb, is also shown in Figure 4. We extended the CRS model to the smaller optical depths needed for our comparison by reference to the Chang *et al.* (1991) calculations. We proceeded by adopting the CRS model and extrapolating their line source function to smaller optical depths by assuming that, at line center, $d \log S / d \log \tau = -0.128$. This gradient was taken from Figure 1 of Chang *et al.* (1991). The actual line profile for these calculations was assumed to be gaussian, with a FWHM of 0.017 cm^{-1}. Because our observations refer to the total intensity in the line, we took the integrated signal in the line. To account for spatial resolution, the resultant limb emission profile was convolved with a rectangular function of 220 km width to simulate the degradation due to lunar topography. The resultant profile is shown as a dashed line on Figure 4. Its sum over height is represented by the dashed line in Figure 3.

4. Results and Discussion

Figure 4 shows that the observed emission profile has a maximum very close to the 12-μm continuum limb, as predicted by theory for an NLTE emission line. The emission peak is not displaced by the approximately 700 km which would be required for an LTE chromospheric emission (Chang *et al.* 1991). On the other

hand, the peak in the emission is not nearly as distinct as predicted by the CRS theory, and the emission extends much higher than calculated from the theory. Using the continuum as a reference, it is possible to compare the magnitude of the observed line energy with theory. The observed line intensity scale on Figure 4 has been expanded by a factor of 10 relative to the continuum scale. Recalling that the continuum refers to the total energy in the 1.0 cm^{-1} bandpass of the array, we see that the observed peak line signal is about 0.7/10 = 7% of the continuum signal, *i.e.*, equal to the energy in 0.07 cm^{-1} of the continuum. Our calculations using the CRS line source function indicate that the line-core-to-continuum specific intensity ratio is $\sim$ 2 just inside the limb, but optical thickness makes the total line energy depend on the form adopted for the line profile. Using a gaussian profile of 0.017 cm^{-1} FWHM we can account for only one-third of the observed line intensity. A better theoretical line shape would place a significant fraction of the opacity in the line wings, thereby giving a greater value for the calculated line intensity. Having no observation of a resolved line profile at the extreme limb, the absolute magnitude of the calculated curves in Figures 3 and 4 is not known, and only their shapes are significant. However, observations on the disk (*e.g.*, Brault and Noyes 1983) imply that the total line intensity above the limb cannot be much greater than the theoretical prediction. The altitude extension we observe does not, therefore, imply that the line contains more emission than predicted, but only that the scale height of the emitting layer is several times greater than in the model.

The good agreement which CRS obtain for the observed profiles of the line at μ = 1.0 and 0.2 shows that their model correctly predicts the dependence of the source function on optical depth, $S(\tau)$. However, the *height* dependence of the emission source function, $S(h)$, is not constrained by comparison with previous observations. The heights from the model are computed under the assumption that the solar atmosphere is in gravitational hydrostatic equilibrium (*e.g.*, Vernazza *et al.* 1981, VAL). Since specification of $S(h)$ is critical to proper interpretation of magnetic data taken using the 12.32 μm line, it would clearly be better to derive it from direct observation. Moreover, an extended infrared limb has been seen before, in the continuum. Eclipse observations in the far-IR continuum have shown that the limb is extended to heights well above the predictions of the VAL model. Lindsey *et al.* (1986) found that the 100- and 200-μm continuum limbs were extended by $\sim$ 1 arcsec above the VAL prediction, implying "large departures from gravitational-hydrostatic equlibrium almost immediately above the chromospheric temperature minimum." Although the 12.32 μm line is photospheric when seen on the disk, the increase in optical depth for the extreme limb-viewing situation means that most of the emission observed here arises from above $T_{\min}$, where such departures occur. This is easily seen by comparing Figure 3 of Chang *et al.* (1991) to the position of $T_{\min}$ in the VAL model. However, the Lindsey *et al.* (1986) results require increases in chromospheric density, and such increases may affect the 12.32-μm emission. In addition, the region above the temperature minimum will probably contain spatial inhomogeneities. Such inhomogeneities will have the effect of extending the emission to greater altitudes when viewed at the extreme limb. This effect is also likely to contribute to the extension which we observe. Full develeopment of theory incorporating departures from hydrostatic equilibrium and spatial inhomogeneities are

needed to fully understand the chromospheric portion of the 12.32-μm emission.

Acknowledgements

We thank the IRTF Director and staff for accommodating this experiment (which placed unusual requirements on the facility), and for their excellent support. We are grateful to Mr. Mark Paules of C. P. Converters for providing the polypropylene plastic used to protect the telescope. Dr. Charles Lindsey made a number of valuable suggestions both before and after the experiment. Dr. Mats Carlsson kindly provided tabulations of the CRS model optical depths and source functions, and Dr. Dennis Reuter assisted in preparing our instrumentation for this experiment. The BIB detector array was supplied by Rockwell International Corporation's Science Center. Celeste was manufactured by IR Systems. The data system and array electronics were fabricated by Electromechanical Design and Fabrication, and Wallace Instruments. This work was supported by the NASA Solar Physics Branch, under RTOP 170-38-53-10, and by the Goddard Director's Discretionary Fund.

References

Brault, J.W., and Noyes, R.W.: 1983, *Astrophys. J. (Letters)* **269**, L61.
Carlsson, M., Rutten, R.J., and Shchukina, N.G. 1992, *Astron. Astrophys.* **253**, 567.
Chang, E.S., and Schoenfeld, W.G. 1991, *Astrophys. J.* **383**, 450.
Chang, E.S., Avrett, E.H., Mauas, P.J., Noyes, R.W., and Loeser, R. 1991, *Astrophys. J.* **379**, 79.
Deming, D., Boyle, R.J., Jennings, D.E., and Wiedemann, G. 1988, *Astrophys. J.* **333**, 978.
Deming, D., Jennings, D.E., McCabe, G., Noyes, R., Wiedemann, G., and Espenak, F. 1992 *Astrophys. J. (Letters)* **396**, L53.
Hoang-Binh, D. 1991 *Astron. Astrophys.* **241**, L13.
Lemke, M., and Holweger, H. 1987 *Astron. Astrophys.* **173**, 375.
Lindsey, C., Becklin, E.E., Orrall, F.Q., Werner, M.W., Jefferies, J.T., and Gatley, I. 1986, *Astrophys. J.* **308**, 448.
Vernazza, J.E., Avrett, E.H., and Loeser, R. 1981 *Astrophys. J. Suppl.* **45**, 635.
Watts, C.B. 1963, *Astron. Papers Amer. Ephem.* **17**, 1.